

Measurements of $\psi(2S)$ decays into $\gamma K \bar{K} \pi$ and $\gamma \eta \pi^+ \pi^-$

M. Ablikim¹, J. Z. Bai¹, Y. Ban¹², J. G. Bian¹, X. Cai¹, H. F. Chen¹⁷, H. S. Chen¹, H. X. Chen¹, J. C. Chen¹, Jin Chen¹, Y. B. Chen¹, S. P. Chi², Y. P. Chu¹, X. Z. Cui¹, Y. S. Dai¹⁹, L. Y. Diao⁹, Z. Y. Deng¹, Q. F. Dong¹⁵, S. X. Du¹, J. Fang¹, S. S. Fang², C. D. Fu¹, C. S. Gao¹, Y. N. Gao¹⁵, S. D. Gu¹, Y. T. Gu⁴, Y. N. Guo¹, Y. Q. Guo¹, Z. J. Guo¹⁶, F. A. Harris¹⁶, K. L. He¹, M. He¹³, Y. K. Heng¹, H. M. Hu¹, T. Hu¹, G. S. Huang^{1a}, X. T. Huang¹³, X. B. Ji¹, X. S. Jiang¹, X. Y. Jiang⁵, J. B. Jiao¹³, D. P. Jin¹, S. Jin¹, Yi Jin⁸, Y. F. Lai¹, G. Li², H. B. Li¹, H. H. Li¹, J. Li¹, R. Y. Li¹, S. M. Li¹, W. D. Li¹, W. G. Li¹, X. L. Li¹, X. N. Li¹, X. Q. Li¹¹, Y. L. Li⁴, Y. F. Liang¹⁴, H. B. Liao¹, B. J. Liu¹, C. X. Liu¹, F. Liu⁶, Fang Liu¹, H. H. Liu¹, H. M. Liu¹, J. Liu¹², J. B. Liu¹, J. P. Liu¹⁸, Q. Liu¹, R. G. Liu¹, Z. A. Liu¹, Y. C. Lou⁵, F. Lu¹, G. R. Lu⁵, J. G. Lu¹, C. L. Luo¹⁰, F. C. Ma⁹, H. L. Ma¹, L. L. Ma¹, Q. M. Ma¹, X. B. Ma⁵, Z. P. Mao¹, X. H. Mo¹, J. Nie¹, S. L. Olsen¹⁶, H. P. Peng^{17b}, R. G. Ping¹, N. D. Qi¹, H. Qin¹, J. F. Qiu¹, Z. Y. Ren¹, G. Rong¹, L. Y. Shan¹, L. Shang¹, C. P. Shen¹, D. L. Shen¹, X. Y. Shen¹, H. Y. Sheng¹, H. S. Sun¹, J. F. Sun¹, S. S. Sun¹, Y. Z. Sun¹, Z. J. Sun¹, Z. Q. Tan⁴, X. Tang¹, G. L. Tong¹, G. S. Varner¹⁶, D. Y. Wang¹, L. Wang¹, L. L. Wang¹, L. S. Wang¹, M. Wang¹, P. Wang¹, P. L. Wang¹, W. F. Wang^{1b}, Y. F. Wang¹, Z. Wang¹, Z. Y. Wang¹, Zhe Wang¹, Zheng Wang², C. L. Wei¹, D. H. Wei¹, N. Wu¹, X. M. Xia¹, X. X. Xie¹, G. F. Xu¹, X. P. Xu⁶, Y. Xu¹¹, M. L. Yan¹⁷, H. X. Yang¹, Y. X. Yang³, M. H. Ye², Y. X. Ye¹⁷, Z. Y. Yi¹, G. W. Yu¹, C. Z. Yuan¹, J. M. Yuan¹, Y. Yuan¹, S. L. Zang¹, Y. Zeng⁷, Yu Zeng¹, B. X. Zhang¹, B. Y. Zhang¹, C. C. Zhang¹, D. H. Zhang¹, H. Q. Zhang¹, H. Y. Zhang¹, J. W. Zhang¹, J. Y. Zhang¹, S. H. Zhang¹, X. M. Zhang¹, X. Y. Zhang¹³, Yiyun Zhang¹⁴, Z. P. Zhang¹⁷, D. X. Zhao¹, J. W. Zhao¹, M. G. Zhao¹, P. P. Zhao¹, W. R. Zhao¹, Z. G. Zhao^{1d}, H. Q. Zheng¹², J. P. Zheng¹, Z. P. Zheng¹, L. Zhou¹, N. F. Zhou^{1c}, K. J. Zhu¹, Q. M. Zhu¹, Y. C. Zhu¹, Y. S. Zhu¹, Yingchun Zhu^{1b}, Z. A. Zhu¹, B. A. Zhuang¹, X. A. Zhuang¹, B. S. Zou¹

(BES Collaboration)

¹ Institute of High Energy Physics, Beijing 100049, People's Republic of China

² China Center for Advanced Science and Technology (CCAST), Beijing 100080, People's Republic of China

³ Guangxi Normal University, Guilin 541004, People's Republic of China

⁴ Guangxi University, Nanning 530004, People's Republic of China

⁵ Henan Normal University, Xinxiang 453002, People's Republic of China

⁶ Huazhong Normal University, Wuhan 430079, People's Republic of China

⁷ Hunan University, Changsha 410082, People's Republic of China

⁸ Jinan University, Jinan 250022, People's Republic of China

⁹ Liaoning University, Shenyang 110036, People's Republic of China

¹⁰ Nanjing Normal University, Nanjing 210097, People's Republic of China

¹¹ Nankai University, Tianjin 300071, People's Republic of China

¹² Peking University, Beijing 100871, People's Republic of China

¹³ Shandong University, Jinan 250100, People's Republic of China

¹⁴ Sichuan University, Chengdu 610064, People's Republic of China

¹⁵ Tsinghua University, Beijing 100084, People's Republic of China

¹⁶ University of Hawaii, Honolulu, HI 96822, USA

¹⁷ University of Science and Technology of China, Hefei 230026, People's Republic of China

¹⁸ Wuhan University, Wuhan 430072, People's Republic of China

¹⁹ Zhejiang University, Hangzhou 310028, People's Republic of China

^a Current address: Purdue University, West Lafayette, IN 47907, USA

^b Current address: DESY, D-22607, Hamburg, Germany

^c Current address: Laboratoire de l'Accélérateur Linéaire, Orsay, F-91898, France

^d Current address: University of Michigan, Ann Arbor, MI 48109, USA

Radiative decays of the $\psi(2S)$ into $\gamma K\bar{K}\pi$ and $\gamma\eta\pi^+\pi^-$ final states are studied using 14 million $\psi(2S)$ events collected with the BESII detector. Branching fractions or upper limits on the branching fractions of $\psi(2S)$ and χ_{cJ} decays are reported. No significant signal for $\eta(1405)/\eta(1475)$ is observed in the $K\bar{K}\pi$ or $\eta\pi^+\pi^-$ mass spectra, and upper limits on the branching fractions of $\psi(2S) \rightarrow \gamma\eta(1405)/\eta(1475)$, $\eta(1405)/\eta(1475) \rightarrow K\bar{K}\pi$ and $\eta\pi^+\pi^-$ are determined.

PACS numbers: 13.25.Gv, 12.38.Qk, 14.40.Gx

I. INTRODUCTION

$\psi(2S)$ decays via three gluons or a single direct photon have been extensively studied [1]. However, there have been fewer studies of $\psi(2S)$ radiative decays [2]. Further study of $\psi(2S)$ radiative decays will provide more information about the $\psi(2S)$ decay mechanism and may help in understanding problems like the “ $\rho\pi$ puzzle”. The “12% rule” predicted by perturbative QCD [3] is expected to be applicable to $\psi(2S)$ radiative decays [4], so it can be tested by measuring more of these decays. Furthermore, if the 12% rule is obeyed for the $\psi(2S) \rightarrow \gamma\eta(1440)$ [2] decay, we might expect to observe $\eta(1440)$ in $\psi(2S)$ decays into $\gamma K\bar{K}\pi$ and $\gamma\eta\pi^+\pi^-$.

A glueball candidate, the $\eta(1440)$, is now regarded as the superposition of two independent states, the $\eta(1405)$ and the $\eta(1475)$, with different decay modes [2]. The $\eta(1475)$ could be the first radial excitation of the $\eta'(958)$, while the $\eta(1295)$ could be the first radial excitation of the η . The results of L3’s measurements on the $K\bar{K}\pi$ and $\eta\pi^+\pi^-$ channels in $\gamma\gamma$ collisions suggest that the $\eta(1405)$ has a large gluonic content [5]. However CLEO did not confirm L3’s results with a five times larger data sample and set upper limits on $\Gamma_{\gamma\gamma}(\eta(1405))\mathcal{B}(\eta(1405) \rightarrow K\bar{K}\pi)$ and $\Gamma_{\gamma\gamma}(\eta(1475))\mathcal{B}(\eta(1475) \rightarrow K\bar{K}\pi)$, which are still consistent with the glueball and the radial excitation hypotheses for $\eta(1405)$ and $\eta(1475)$ [6].

Many studies have been made for $\eta(1405)/\eta(1475)$ with J/ψ decays into $K\bar{K}\pi$, $\eta\pi^+\pi^-$, 4π , and $\gamma\rho^0$ [2], while in $\psi(2S)$ decay, only MARKI reported an upper limit at the 90% confidence level (C.L.) for $\psi(2S) \rightarrow \gamma\eta(1405) \rightarrow \gamma K\bar{K}\pi$ [7]. Here we study $\eta(1405)/\eta(1475)$ in $\psi(2S)$ radiative decays to $\gamma K\bar{K}\pi$ and $\gamma\eta\pi^+\pi^-$ final states using a sample of 14×10^6 $\psi(2S)$ events.

In lowest-order perturbative QCD, the χ_{c0} and χ_{c2} decay via the annihilation of their constituent $c\bar{c}$ quarks into two gluons, followed by hadronization of the gluons into light mesons and baryons, so these decays are expected to be similar to those of a gg bound state, while χ_{c1} cannot decay via the annihilation of their constituent $c\bar{c}$ quarks into two gluons. So systematic and detailed studies of hadronic decays of the

χ_{cJ} may help in understanding the decay patterns of glueball states that will be helpful for their identification.

BESI collaboration studied χ_{cJ} decays into $K_S^0 K^+\pi^- + c.c.$ [8] and reported χ_{c1} branching fractions and upper limits on branching fractions of χ_{c0} and χ_{c2} decays. In this paper, we report measurements of $\psi(2S)$ decays into $\gamma K\bar{K}\pi$ and $\gamma\eta\pi^+\pi^-$ final states using 14 million $\psi(2S)$ events collected with the BESII detector. With about a four times larger $\psi(2S)$ sample, more precise results are expected. Branching fractions or upper limits of $\psi(2S)$ and χ_{cJ} decays are reported.

II. THE BESII DETECTOR

The Beijing Spectrometer (BESII) is a conventional cylindrical magnetic detector that is described in detail in Ref. [9]. A 12-layer vertex chamber (VC) surrounding the beryllium beam pipe provides input to the event trigger, as well as coordinate information. A forty-layer main drift chamber (MDC) located just outside the VC yields precise measurements of charged particle trajectories with a solid angle coverage of 85% of 4π ; it also provides ionization energy loss (dE/dx) measurements which are used for particle identification. Momentum resolution of $1.7\%\sqrt{1+p^2}$ (p in GeV/ c) and dE/dx resolution for hadron tracks of $\sim 8\%$ are obtained. An array of 48 scintillation counters surrounding the MDC measures the time of flight (TOF) of charged particles with a resolution of about 200 ps for hadrons. Outside the TOF counters, a 12 radiation length, lead-gas barrel shower counter (BSC), operating in limited streamer mode, measures the energies of electrons and photons over 80% of the total solid angle with an energy resolution of $\sigma_E/E = 0.22/\sqrt{E}$ (E in GeV). A solenoidal magnet outside the BSC provides a 0.4 T magnetic field in the central tracking region of the detector. Three double-layer muon counters instrument the magnet flux return and serve to identify muons with momentum greater than 500 MeV/ c . They cover 68% of the total solid angle.

III. EVENT SELECTION

The decay channels investigated in this paper are $\psi(2S) \rightarrow \gamma K_S^0 K^+ \pi^- + c.c.$, $\gamma K^+ K^- \pi^0$ and $\gamma \eta \pi^+ \pi^-$, where K_S^0 decays to $\pi^+ \pi^-$, η to $\gamma \gamma$, and π^0 to $\gamma \gamma$.

A neutral cluster is considered to be a photon candidate if the following requirements are satisfied: it is located within the BSC fiducial region, the energy deposited in the BSC is greater than 50 MeV, the first hit appears in the first 6 radiation lengths, the angle in the xy plane (perpendicular to the beam direction) between the cluster and the nearest charged track is greater than 8° , and the angle between the cluster development direction in the BSC and the photon emission direction from the beam interaction point (IP) is less than 37° .

Each charged track is required to be well fitted by a three-dimensional helix, to have a momentum transverse to the beam direction greater than 70 MeV/c, to originate from the IP region ($V_{xy} = \sqrt{V_x^2 + V_y^2} < 2$ cm and $|V_z| < 20$ cm) if it is not from K_S^0 decay, and to have a polar angle $|\cos \theta| < 0.8$. Here V_x , V_y , and V_z are the x , y , and z coordinates of the point of closest approach of the track to the beam axis.

The TOF and dE/dx measurements for each charged track are used to calculate $\chi_{PID}^2(i)$ values and the corresponding confidence levels $Prob_{PID}(i)$ for the hypotheses that a track is a pion, kaon, or proton, where i ($i = \pi/K/p$) is the particle type. For each event, charged kaon candidates are required to have $Prob_{PID}(K)$ larger than 0.01, while charged pion candidates are required to have $Prob_{PID}(\pi) > 0.01$.

IV. EVENT ANALYSIS

A. $\psi(2S) \rightarrow \gamma K_S^0 K^+ \pi^- + c.c.$

For the final state $\gamma K^\pm \pi^\mp \pi^+ \pi^-$, the candidate events are required to have at least one photon candidate and four good charged tracks with net charge zero. A four constraint (4C) kinematic fit is performed to the hypothesis $\psi(2S) \rightarrow \gamma K^\pm \pi^\mp \pi^+ \pi^-$, and the χ^2 of the fit is required to be less than 15. If there is more than one photon, the fit is performed with the photon candidate which has the largest energy deposit in the BSC. A 4C-fit to the hypothesis $\psi(2S) \rightarrow \gamma \pi^+ \pi^- \pi^+ \pi^-$ is also performed, and $\chi_{4C}^2(\gamma K^\pm \pi^\mp \pi^+ \pi^-) < \chi_{4C}^2(\gamma \pi^+ \pi^- \pi^+ \pi^-)$ is required to suppress background from $\gamma \pi^+ \pi^- \pi^+ \pi^-$.

Backgrounds from $\psi(2S) \rightarrow \pi^+ \pi^- J/\psi$ are rejected with the requirement $|m_{recoil}^{\pi^+ \pi^-} - 3.1| > 0.05$ GeV/c²,

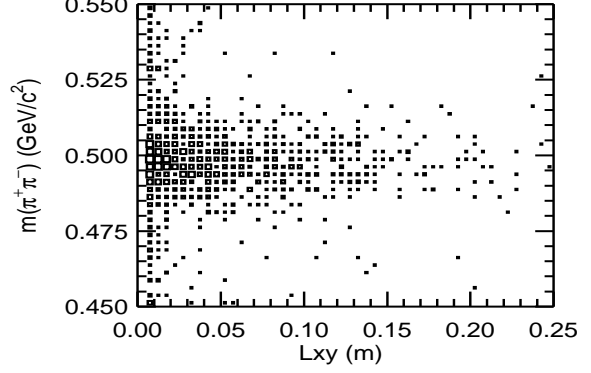


FIG. 1: The scatter plot of $\pi^+ \pi^-$ invariant mass versus the K_S^0 decay length.

where $m_{recoil}^{\pi^+ \pi^-}$ is the mass recoiling from each possible $\pi^+ \pi^-$ pair. Figure 1 shows the scatter plot of $\pi^+ \pi^-$ invariant mass versus the decay length in the transverse plane (L_{xy}) of K_S^0 candidates. A clear K_S^0 signal is observed. Candidate events are required to have only one K_S^0 candidate satisfying the requirements $|m_{\pi^+ \pi^-} - 0.498| < 0.015$ GeV/c² and $L_{xy} > 0.5$ cm. After K_S^0 selection, if one of the remaining tracks has a momentum higher than 1.5 GeV/c, it is taken as a charged kaon. Otherwise, the track types are selected using their $\chi_{K\pi}^2$ values, *i.e.*, if $\chi_{K^+ \pi^-}^2 < \chi_{\pi^+ K^-}^2$, the final state is considered to be $\gamma K_S^0 K^+ \pi^-$; if $\chi_{K^- \pi^+}^2 < \chi_{\pi^- K^+}^2$, the final state is considered to be $\gamma K_S^0 K^- \pi^+$, where $\chi_{K\pi}^2 = \chi_{PID}^2(K) + \chi_{PID}^2(\pi)$.

With this selection, Fig. 2 shows the mass distribution of $K_S^0 K^+ \pi^-$ and $K_S^0 K^- \pi^+$ for candidate events. There is a clear χ_{c1} signal, but no clear $\eta(1405)/\eta(1475)$ signal. The biggest background contamination comes from $\psi(2S) \rightarrow \pi^0 K_S^0 K^+ \pi^- + c.c.$, which is estimated with the data sample, and the other backgrounds are estimated by Monte Carlo (MC) simulation.

In the high mass region, the fit of the $K_S^0 K^+ \pi^- + c.c.$ invariant mass spectrum is performed after subtracting the known background, and a second order polynomial is used to describe the shape of the remaining unknown background (see Fig. 3). The χ_{c0} peak is described with a Breit-Wigner folded with a double-Gaussian resolution function determined from MC simulation, while the χ_{c1} and χ_{c2} peaks are described only with double-Gaussians resolution functions because their widths are much smaller than the mass resolution. The masses of the three χ_{cJ} states and the width of χ_{c0} are fixed to PDG values [2].

A binned maximum likelihood method is used to fit all events with $K_S^0 K^\pm \pi^\mp$ mass between 3.2 and 3.65 GeV/c². The numbers of events are 3.9 ± 4.6 ,

220 ± 16 , and 28.4 ± 7.6 with statistical significances of 0.9σ , 22.0σ , and 4.8σ [10] for χ_{c0} , χ_{c1} , and χ_{c2} , respectively.

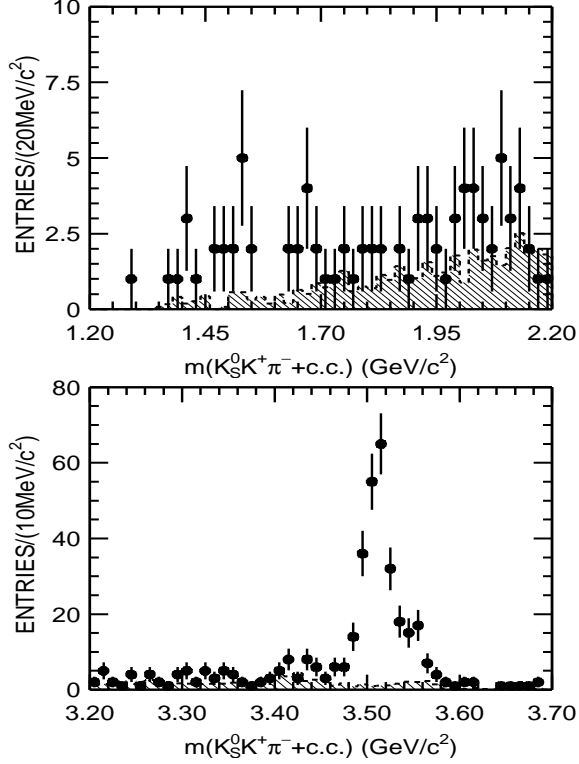


FIG. 2: Invariant mass distributions for $\psi(2S) \rightarrow K_S^0 K^+ \pi^- + c.c.$ candidate events in the low mass region (upper plot) and high mass region (lower). Dots with error bars are data, and the hatched histogram is simulated background.

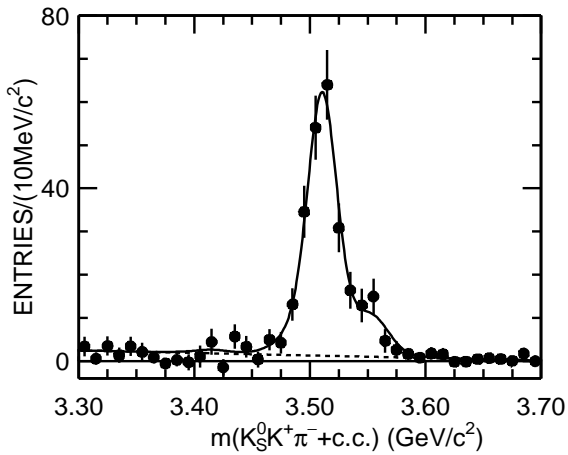


FIG. 3: The result of the $K_S^0 K^+ \pi^- + c.c.$ mass fit. The curve shows the best fit described in the text.

Figure 4(a) shows the Dalitz plot of $\chi_{c1} \rightarrow K_S^0 K^+ \pi^- + c.c.$ candidate events with $3.48 \text{ GeV}/c^2 < m_{K_S^0 K^\pm \pi^\mp} < 3.53 \text{ GeV}/c^2$. The clusters of events indicate $K^*(892)$ and $K_J^*(1430)$ signals. Figure 4(b)

shows the $K^\pm \pi^\mp$ invariant mass distribution after an additional requirement $m_{K_S^0 \pi^\pm} > 1.0 \text{ GeV}/c^2$ to reject $K^{*\pm} K^\mp$ events. Figure 4(c) shows the $K_S^0 \pi^\pm$ invariant mass after the requirement $m_{K^\pm \pi^\mp} > 1.0 \text{ GeV}/c^2$ to reject $K^{*0} \bar{K}^0$ events.

For $\chi_{c1} \rightarrow K_S^0 K^+ \pi^- + c.c.$ candidate events, the $K^\pm \pi^\mp$ and $K_S^0 \pi^\pm$ mass spectra are fitted with $K^*(892)$ and $K_J^*(1430)$ signal shapes determined from MC simulations plus a threshold function for background. For $K^*(892)^0$ and $K^*(892)^\pm$, the fitted numbers of events are 22.5 ± 7.3 and 26.7 ± 11.0 with corresponding statistical significances of 3.5σ and 3.0σ , respectively. For $K_J^*(1430)$, there are three states: $K_2^*(1430)$, $K_0^*(1430)$, and $K^*(1410)$ around $1430 \text{ MeV}/c^2$. With the detection efficiencies averaged with equal weight, the numbers of events including these three hypotheses are calculated to be 22 ± 15 and 45 ± 26 for $K_J^*(1430)^0$ and $K_J^*(1430)^\pm$, respectively [11]. The upper limits on the numbers of events at the 90% C.L. are calculated to be 41 and 79.

In the low mass region, no $\eta(1405)/\eta(1475)$ signal is observed in the $K_S^0 K^\pm \pi^\mp$ invariant mass distribution. Here the fit is performed under two hypotheses: one for $\eta(1405)$ with mass $1410 \text{ MeV}/c^2$, width $51 \text{ MeV}/c^2$, and mass resolution $7.1 \text{ MeV}/c^2$; the other for $\eta(1475)$ with mass $1476 \text{ MeV}/c^2$, width $87 \text{ MeV}/c^2$, and mass resolution $7.7 \text{ MeV}/c^2$. The $K_S^0 K^+ \pi^- + c.c.$ invariant mass distribution is fitted with a Breit-Wigner folded with a Gaussian resolution and a second order polynomial for background. The mass, width, and mass resolution are fixed to the values above. The signal is very weak, so upper limits on the number of events are calculated to be 11 and 16 for $\eta(1405)$ and $\eta(1475)$, respectively.

B. $\psi(2S) \rightarrow \gamma K^+ K^- \pi^0$

For this channel, candidate events are required to have two charged tracks with net charge zero and three photon candidates. A 4C-fit is performed under the $\psi(2S) \rightarrow \gamma\gamma K^+ K^-$ hypothesis, and the χ^2 of the fit is required to be less than 15. The invariant mass of the charged kaon tracks is required to be less than $3.0 \text{ GeV}/c^2$ to veto $\psi(2S) \rightarrow \text{neutral} + J/\psi$ background. With three selected photons, there are three possible combinations to reconstruct π^0 , and the combination with invariant mass closest to m_{π^0} is taken as the π^0 candidate. Figure 5 shows the $\gamma\gamma$ invariant mass distribution, where a clear π^0 signal is observed.

After requiring $|m_{\gamma\gamma} - m_{\pi^0}| < 0.03 \text{ GeV}/c^2$, Fig. 6 shows the $K^+ K^- \pi^0$ mass distribution for candidate events. There is no $\eta(1405)/\eta(1475)$ signal in the low

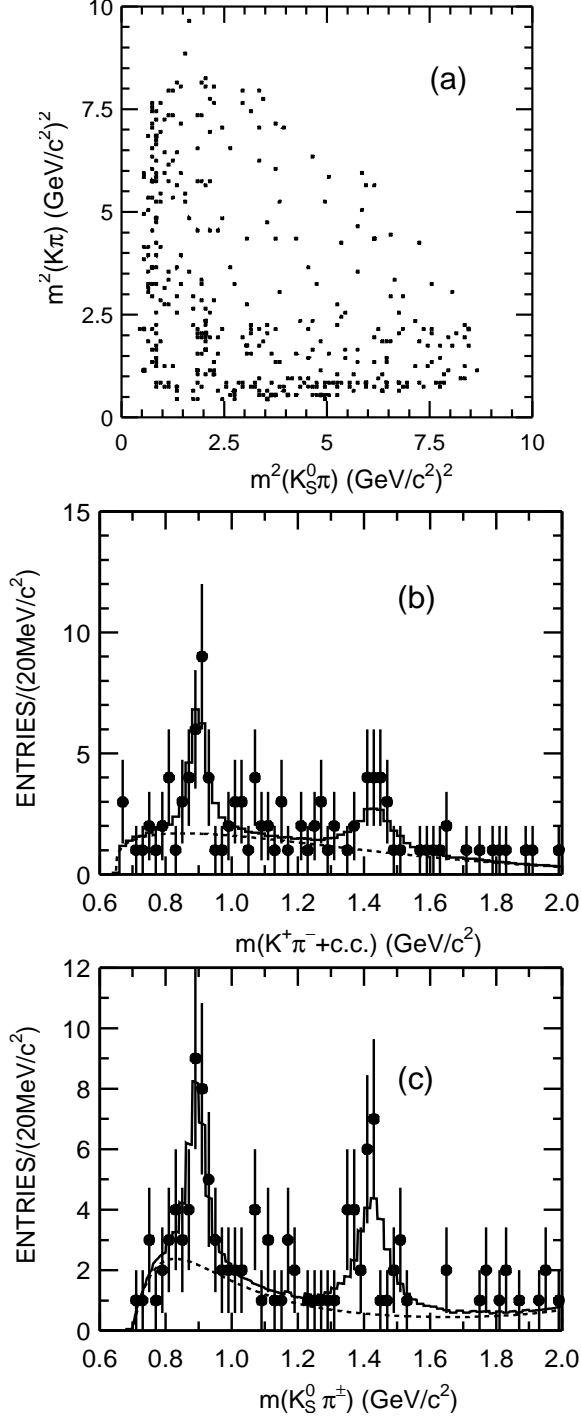


FIG. 4: (a) Dalitz plot of $\chi_{c1} \rightarrow K_S^0 K^+ \pi^- + c.c.$ candidate events. The (b) $K^\pm \pi^\mp$ and (c) $K_S^0 \pi^\pm$ invariant mass distributions. In (b) and (c), dots with error bars are data, and the histograms show the best fits described in the text.

mass region. Upper limits on the number of events are calculated to be 9 and 9 for $\eta(1405)$ and $\eta(1475)$, respectively.

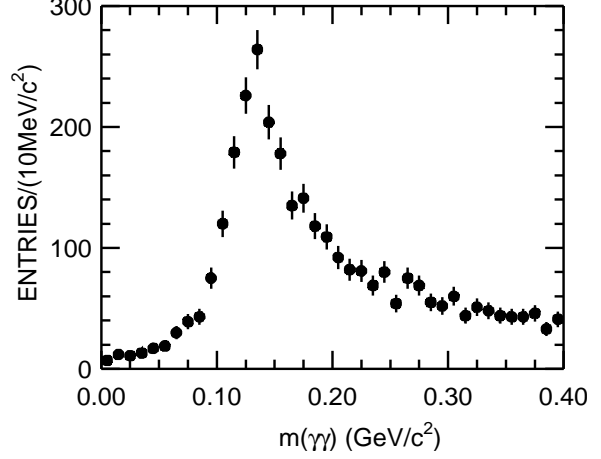


FIG. 5: The $\gamma\gamma$ invariant mass distribution for $\psi(2S) \rightarrow \gamma\gamma K^+ K^-$ candidate events.

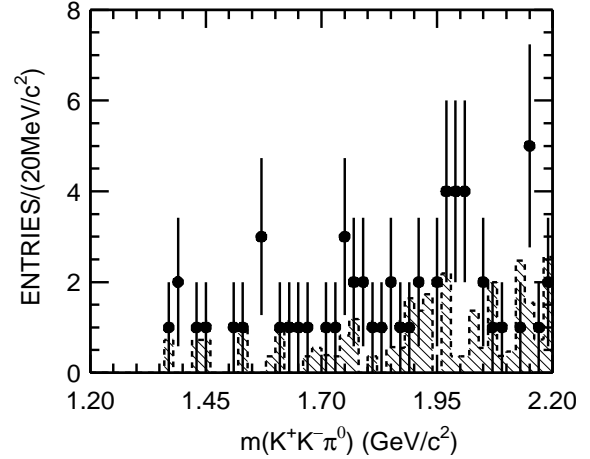


FIG. 6: The $K^+ K^- \pi^0$ invariant mass distribution for $\psi(2S) \rightarrow \gamma K^+ K^- \pi^0$ candidate events. Dots with error bars are data, and the hatched histogram is the simulated background.

C. $\psi(2S) \rightarrow \gamma \eta \pi^+ \pi^-$

The final state of this channel is $\pi^+ \pi^- \gamma \gamma$. Events with two charged tracks with net charge zero and three photon candidates are selected. A 4C-fit is performed for the hypothesis $\psi(2S) \rightarrow \pi^+ \pi^- \gamma \gamma$, and the χ^2 of the fit is required to be less than 15. Background from $\psi(2S) \rightarrow \pi^+ \pi^- J/\psi$ is rejected with the requirement $|m_{recoil}^{\pi^+ \pi^-} - 3.1| > 0.05 \text{ GeV}/c^2$. Background from $\psi(2S) \rightarrow \text{neutrals} + J/\psi$ is suppressed with the requirement $m_{\gamma \pi^+ \pi^-} < 2.8 \text{ GeV}/c^2$, where $m_{\gamma \pi^+ \pi^-}$ is the invariant mass of the $\pi^+ \pi^-$ and the photon which does not come from η decay.

With the above selection, Fig. 7 shows the $\gamma\gamma$ invariant mass distribution, where $\gamma\gamma$ includes all possible combinations among the three photon candidates. A clear η signal is observed. The smooth background

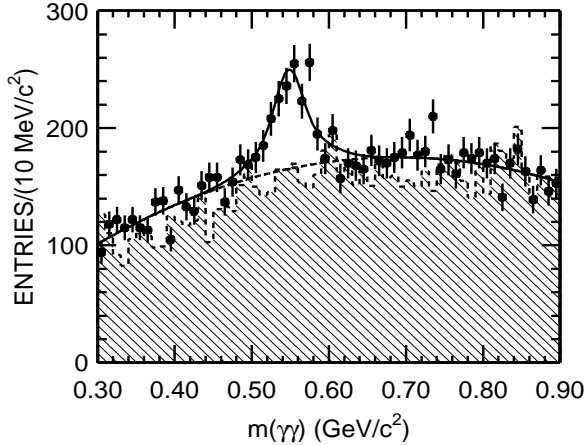


FIG. 7: The $\gamma\gamma$ invariant mass distribution for $\psi(2S) \rightarrow \pi^+\pi^-\gamma\gamma$ candidate events (dots with error bars). The curves show the best fit described in the text. The hatched histogram is the $\gamma\gamma$ distribution of background events from the continuum and the 14M inclusive decay MC sample with signal events removed.

comes from many channels and can be described by the sum of continuum events and $\psi(2S)$ inclusive decay MC events, where the signal events have been removed and some known background channels are replaced by MC simulated results. The main background of the η signal comes from $\psi(2S) \rightarrow \eta\pi^+\pi^-\pi^0$, which is estimated using $\psi(2S)$ data. We also studied other possible channels listed in the PDG [2] that might contaminate the η signal, but the contamination is negligible. A fit of the $m_{\gamma\gamma}$ spectrum yields 553 ± 60 events, and the background contamination is estimated to be 135 ± 59 by fitting the hatched histogram in Fig. 7. In the fit, the η signal is described by the double-Gaussian shape determined from $\psi(2S) \rightarrow \gamma\eta\pi^+\pi^-$ MC simulation. After the background contamination is subtracted, the number of η events is 418 ± 60 , with a statistical significance of 7.3σ . Here the background contamination is subtracted from the total number of observed events, and the uncertainty on the number of background events is taken as a systematic error. This method to deal with the background contamination is also applied to the following analyses.

An η candidate is defined with the requirement $|m_{\gamma\gamma} - 0.548| < 0.04 \text{ GeV}/c^2$. Figure 8 shows the $\eta\pi^+\pi^-$ invariant mass distributions in the low and high mass regions. Clear $\eta'(958)$ and χ_{c1} signals are seen.

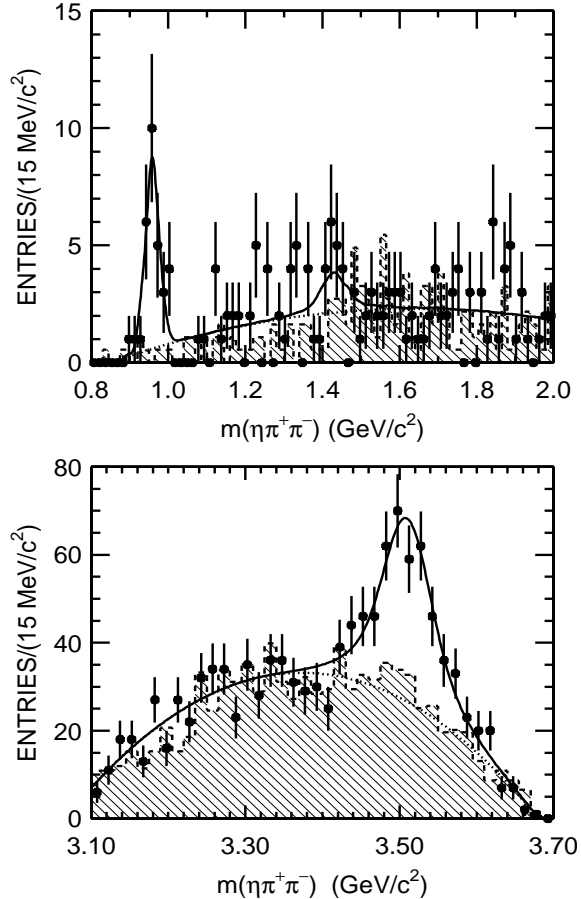


FIG. 8: The $\eta\pi^+\pi^-$ invariant mass distributions for $\psi(2S) \rightarrow \gamma\eta\pi^+\pi^-$ candidate events in the low mass region (upper plot) and high mass region (lower). The dots with error bars are data, and the hatched histogram is the background estimated from the η sidebands. The curves show the best fit described in the text.

1. $\psi(2S) \rightarrow \gamma\eta'(958)$ and $\gamma\eta(1405)/\eta(1475)$

Besides the $\eta'(958)$ signal, there is also a small peak at $1430 \text{ MeV}/c^2$, which could be an $\eta(1405)$, $f_1(1420)$, $\rho(1450)$, or $\eta(1475)$ listed by PDG [2]. $f_1(1420)$ and $\eta(1475)$ dominantly decay into $K\bar{K}\pi$, but no significant signal of $f_1(1420)$ or $\eta(1475)$ is observed in the $K_S K \pi$ invariant mass distribution (see Fig. 2(a)). The $\psi(2S) \rightarrow \gamma\rho(1450)$ decay is forbidden by C-parity conservation. So the peak at $1430 \text{ MeV}/c^2$ is assumed to be $\eta(1405)$ signal, and more will be discussed later.

Assuming $\eta'(958)$ and $\eta(1405)$ signals, the low mass region is fitted with the MC distributions plus a second order polynomial for background (see Fig. 8). The fit yields 24.2 ± 5.4 and 13.8 ± 7.0 events, and the peaking background events are estimated to be 0.9 ± 1.4 and 4.0 ± 4.5 from η sidebands. The η sideband region is defined by $|m_{\gamma\gamma} - 0.38| < 0.04 \text{ GeV}/c^2$ and $|m_{\gamma\gamma} - 0.72| < 0.04 \text{ GeV}$. After background sub-

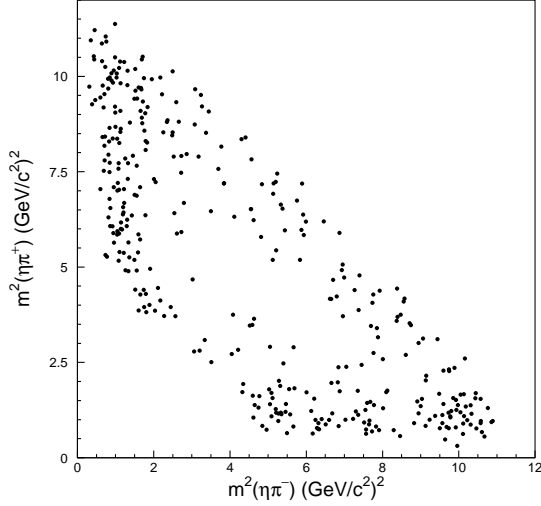


FIG. 9: Dalitz plot of $\chi_{c1} \rightarrow \eta\pi^+\pi^-$ candidate events.

traction, the numbers of $\eta'(958)$ and $\eta(1405)$ events become 23 ± 5 and 10 ± 7 , and the statistical significances are 6.6σ and 1.4σ , respectively.

Since the significance of $\eta(1405)$ is low and there is no clear $\eta(1475)$ signal, upper limits at the 90% C.L. on the numbers of events for $\eta(1405)$ and $\eta(1475)$ are calculated to be 24 and 20, respectively.

2. $\psi(2S) \rightarrow \gamma\chi_{c1}$

The fit in the high $m_{\eta\pi^+\pi^-}$ region yields 256 ± 28 χ_{c1} events (see Fig. 8), and the peaking background events are estimated to be 34 ± 15 from the η sideband region. The η sideband region is defined by $|m_{\gamma\gamma} - 0.38| < 0.04$ GeV/ c^2 and $|m_{\gamma\gamma} - 0.72| < 0.04$ GeV. After the background contamination is subtracted, the number of χ_{c1} signal events becomes 222 ± 28 , with 8.8σ statistical significance.

The Dalitz plot of $\chi_{c1} \rightarrow \eta\pi^+\pi^-$ candidate events within the χ_{c1} mass window (3.46-3.56) GeV/ c^2 is shown in Fig. 9. The horizontal and vertical clusters with $m_{\eta\pi}$ around 1 GeV/ c^2 correspond to $\chi_{c1} \rightarrow a_0(980)\pi$, and the diagonal band is $\chi_{c1} \rightarrow f_2(1270)\pi$.

The $a_0(980)^\pm\pi^\mp$ invariant mass distribution for events satisfying ($|m_{\eta\pi^\pm} - 0.985| < 0.1$ GeV/ c^2) is shown in Fig 10. The distribution is fitted with a MC determined double-Gaussian function plus a second order polynomial for the background. The fit yields 79 ± 14 χ_{c1} candidate events, and the number of background events contributing to the peak is estimated

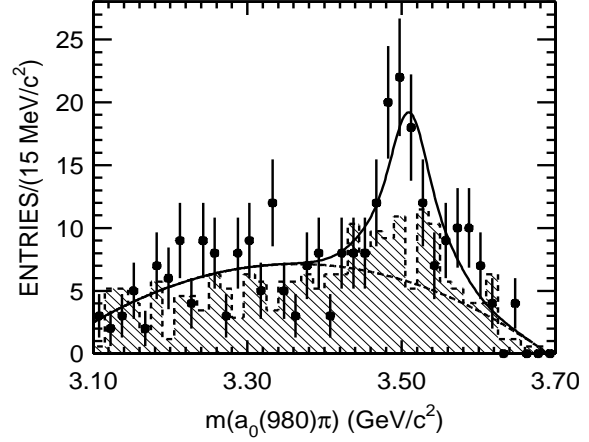


FIG. 10: The $a_0^\pm\pi^\mp$ invariant mass distribution for $\psi(2S) \rightarrow \gamma a_0(980)^\pm\pi^\mp$ candidate events (dots with error bars). The curves show the best fit described in the text. The hatched histogram is the $m_{\eta\pi^+\pi^-}$ distribution of the events in $a_0(980)$ sideband region.

to be 21 ± 11 by using a similar fit for events from the $a_0(980)$ sideband region. The $a_0(980)$ sideband region is defined by $|m_{\eta\pi^\pm} - 1.6| < 0.3$ GeV/ c^2 . After subtraction, the number of χ_{c1} signal events is determined to be 58 ± 14 , with a 4.5σ statistical significance.

Figure 11 shows the scatter plot of $m_{\gamma\gamma}$ versus $m_{\pi^+\pi^-}$ of the χ_{c1} candidate events. The $f_2(1270)\eta$ signal region is defined by $|m_{\pi^+\pi^-} - 1.275| < 0.185$ GeV/ c^2 and $|m_{\gamma\gamma} - 0.548| < 0.04$ GeV/ c^2 . The $f_2(1270)$ sideband region is defined by $|m_{\pi^+\pi^-} - 0.7| < 0.185$ GeV/ c^2 and $|m_{\pi^+\pi^-} - 1.85| < 0.185$ GeV/ c^2 , and the η sideband region by $|m_{\gamma\gamma} - 0.38| < 0.04$ GeV/ c^2 and $|m_{\gamma\gamma} - 0.72| < 0.04$ GeV (see Fig. 11). The central box in the figure is the signal region, the two boxes located above and below the signal region are the η sidebands (named B_η^1 and B_η^2), and the two on the left and right of the signal region are the $f_2(1270)$ sidebands (named $B_{f_2}^1$ and $B_{f_2}^2$). The four boxes at the corners are used to estimate the phase space contribution (named $B_{ph}^i, i = 1, 2, 3, 4$). We use the formula:

$$\frac{1}{2} \times (B_\eta^1 + B_\eta^2 + B_{f_2}^1 + B_{f_2}^2) - \frac{1}{4} \times (B_{ph}^1 + B_{ph}^2 + B_{ph}^3 + B_{ph}^4)$$

to obtain the $m_{\eta\pi^+\pi^-}$ distribution of the events in the sideband regions. Figure 12 shows the $\eta\pi^+\pi^-$ invariant mass distributions of the signal and background regions, and a clear χ_{c1} signal is observed.

The χ_{c1} signal is fitted with a double-Gaussian function determined from MC simulation plus a second order polynomial to describe the background (see Fig. 12). The fit yields 65 ± 13 events, and fitting the sideband region events yields 12 ± 7 sideband background

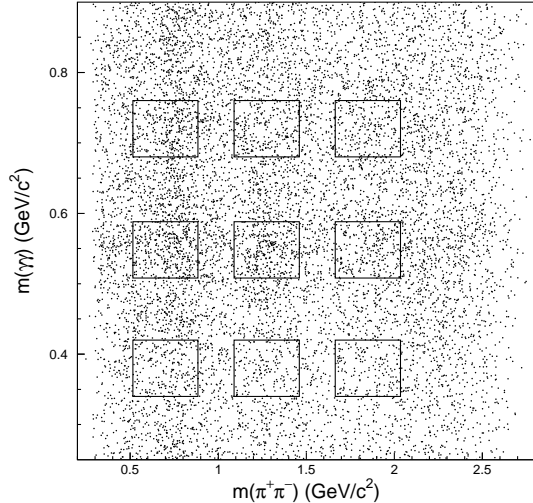


FIG. 11: The scatter plot of $m_{\gamma\gamma}$ versus $m_{\pi^+\pi^-}$ for candidate events.

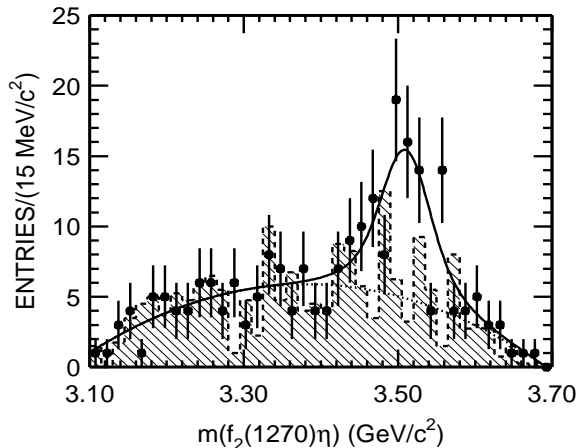


FIG. 12: Invariant mass distribution of $f_2(1270)\eta$ for $\psi(2S) \rightarrow \gamma f_2(1270)\eta$ candidate events (dots with error bars). The curves show the best fit described in the text. The hatched histogram is the $m_{\gamma\pi^+\pi^-}$ distribution of events in the sideband regions.

events. After subtraction, the number of χ_{c1} signal events is 53 ± 13 with a 4.8σ statistical significance.

χ_{c1} decays to $a_0^\pm \pi^\mp$ and $f_2(1270)\eta$ yield the same final state $\eta\pi^+\pi^-$. MC studies show that the sideband analysis described above separates the two channels without cross contamination. However, any interference effects are not taken into consideration because of the low statistics.

V. SIMULATION AND EFFICIENCY

Monte Carlo simulation is used for mass resolution and detection efficiency determination. In this analysis, a GEANT3 based Monte Carlo package with detailed consideration of the detector performance (such as dead electronic channels) is used. The consistency between data and Monte Carlo has been carefully checked in many high purity physics channels, and the agreement is reasonable [12].

For $\psi(2S) \rightarrow \gamma\eta'(958)$ and $\psi(2S) \rightarrow \gamma\eta(1405/1475)$, the photons are distributed according to a $1 + \cos^2\theta$ distribution. For $\psi(2S) \rightarrow \gamma\chi_{cJ}$ under the assumption that the processes are pure E1 transitions [13], the photons are generated as $1 + \cos^2\theta$, $1 - \frac{1}{3}\cos^2\theta$, and $1 + \frac{1}{13}\cos^2\theta$ for χ_{c0} , χ_{c1} , and χ_{c2} , respectively. Multihadronic decays of $\eta'(958)$, $\eta(1405/1475)$, and χ_{cJ} are simulated using phase space distributions.

In the MC simulation for $\psi(2S) \rightarrow \gamma\chi_{c1}$, $\chi_{c1} \rightarrow a_0^\pm \pi^\mp$, the width of $a_0(980)$ is assumed to be 75 MeV/c² in the determination of the detection efficiency. The uncertainty of the efficiency due to the uncertainty of the $a_0(980)$ width is taken as a systematic error in the branching fraction of $\chi_{c1} \rightarrow a_0^\pm \pi^\mp$.

The efficiencies for the determination of the branching fractions of $\psi(2S) \rightarrow \gamma\eta\pi^+\pi^-$, $\chi_{c1} \rightarrow \eta\pi^+\pi^-$ and $\chi_{c1} \rightarrow K_S^0 K^+\pi^- + c.c.$ are determined from a weighted average over the intermediate processes.

VI. SYSTEMATIC ERRORS

Many sources of systematic error are considered. Systematic errors associated with the MDC tracking, kinematic fitting, particle identification, and photon selection efficiencies are determined by comparing J/ψ and $\psi(2S)$ data and Monte Carlo simulation for pure data samples, such as $\psi(2S) \rightarrow \pi^+\pi^- J/\psi$.

The uncertainties on the total number of $\psi(2S)$ events, the branching fractions of intermediate states, the $a_0(980)$ width, the detection efficiency, the background contamination, and the fitting on the mass spectrum are also considered as systematic errors. Table I summarizes the systematic errors for all channels.

VII. RESULTS AND DISCUSSION

Tables II, III, and IV summarize the results for the channels measured in this analysis. Table II lists the branching fractions of $\psi(2S)$ decays. To compare with the 12% rule, Table II also includes the

TABLE I: Summary of systematic errors (%). MDC, 4C, PID, γ eff., $N_{\psi(2S)}$, Int., MC, Bg., Fit. and K_S^0 rec. are for tracking, kinematic fit, particle identification, γ detection efficiency, $\psi(2S)$ total number, the branching fractions of the intermediate states, MC statistics, background, fitting on mass spectrum and K_S^0 reconstruction, respectively.

| Channel ($\psi(2S) \rightarrow$) | MDC | 4C | PID | γ eff. | $N_{\psi(2S)}$ | Int. | MC | Bg. | Fit. | K_S^0 rec. | Total |
|--|-----|-----|-----|---------------|----------------|------|-----|------|------|--------------|-------|
| $\gamma\chi_{c0} \rightarrow \gamma K_S^0 K^+ \pi^- + c.c.$ | 8.0 | 6.0 | - | 2.0 | 4.0 | 8.1 | 1.3 | 20.6 | 18.0 | 3.4 | 30.8 |
| $\gamma\chi_{c1} \rightarrow \gamma K_S^0 K^+ \pi^- + c.c.$ | 8.0 | 6.0 | - | 2.0 | 4.0 | 9.5 | 1.3 | 0.2 | 0.7 | 3.4 | 15.0 |
| $\gamma\chi_{c2} \rightarrow \gamma K_S^0 K^+ \pi^- + c.c.$ | 8.0 | 6.0 | - | 2.0 | 4.0 | 9.4 | 1.3 | 2.9 | 3.9 | 3.4 | 15.7 |
| $\gamma\chi_{c1} \rightarrow \gamma K^*(892)^0 K_S^0$ | 8.0 | 6.0 | - | 2.0 | 4.0 | 9.5 | 1.3 | - | 1.9 | 3.4 | 15.1 |
| $\gamma\chi_{c1} \rightarrow \gamma K^*(892)^\pm K^\mp$ | 8.0 | 6.0 | - | 2.0 | 4.0 | 9.5 | 1.3 | - | 3.2 | 3.4 | 15.3 |
| $\gamma\chi_{c1} \rightarrow \gamma K_J^*(1430)^0 K_S^0 \rightarrow \gamma K_S^0 K^+ \pi^- + c.c.$ | 8.0 | 6.0 | - | 2.0 | 4.0 | 9.5 | 1.3 | - | 5.9 | 3.4 | 16.1 |
| $\gamma\chi_{c1} \rightarrow \gamma K_J^*(1430)^\pm K^\mp \rightarrow \gamma K_S^0 K^+ \pi^- + c.c.$ | 8.0 | 6.0 | - | 2.0 | 4.0 | 9.5 | 1.3 | - | 15.2 | 3.4 | 21.4 |
| $\gamma\eta(1405) \rightarrow \gamma K_S^0 K^+ \pi^- + c.c.$ | 8.0 | 6.0 | - | 2.0 | 4.0 | - | 1.5 | - | 5.0 | 3.4 | 12.6 |
| $\gamma\eta(1475) \rightarrow \gamma K_S^0 K^+ \pi^- + c.c.$ | 8.0 | 6.0 | - | 2.0 | 4.0 | - | 1.5 | - | 24.0 | 3.4 | 26.7 |
| $\gamma\eta(1405) \rightarrow \gamma K^+ K^- \pi^0$ | 4.0 | 4.0 | 2.0 | 6.0 | 4.0 | - | 1.7 | - | 12.3 | - | 15.6 |
| $\gamma\eta(1475) \rightarrow \gamma K^+ K^- \pi^0$ | 4.0 | 4.0 | 2.0 | 6.0 | 4.0 | - | 1.7 | - | 20.0 | - | 22.2 |
| $\gamma\eta\pi^+\pi^-$ | 4.0 | 4.0 | 2.0 | 6.0 | 4.0 | 0.7 | 2.3 | 14.0 | 7.7 | - | 18.7 |
| $\gamma\eta'(958)$ | 4.0 | 4.0 | 2.0 | 6.0 | 4.0 | 3.5 | 1.6 | 6.0 | 2.9 | - | 12.1 |
| $\gamma\eta(1405) \rightarrow \gamma\eta\pi^+\pi^-$ | 4.0 | 4.0 | 2.0 | 6.0 | 4.0 | 0.7 | 1.8 | - | 10.9 | - | 14.5 |
| $\gamma\eta(1475) \rightarrow \gamma\eta\pi^+\pi^-$ | 4.0 | 4.0 | 2.0 | 6.0 | 4.0 | 0.7 | 2.0 | - | 10.0 | - | 13.9 |
| $\gamma\chi_{c1} \rightarrow \gamma\eta\pi^+\pi^-$ | 4.0 | 4.0 | 2.0 | 6.0 | 4.0 | 9.5 | 1.1 | 6.7 | 6.4 | - | 16.3 |
| $\gamma\chi_{c1} \rightarrow \gamma a_0(980)^+ \pi^- + c.c.$ | 4.0 | 4.0 | 2.0 | 6.0 | 4.0 | 14.4 | 1.0 | 19.2 | 6.2 | - | 26.5 |
| $\gamma\chi_{c1} \rightarrow \gamma f_2(1270)\eta$ | 4.0 | 4.0 | 2.0 | 6.0 | 4.0 | 10.0 | 1.0 | 13.2 | 2.8 | - | 19.3 |

TABLE II: Measured branching fractions and upper limits (90% C.L.) for $\psi(2S)$ decays. Results for corresponding J/ψ decays [2] and the ratio $Q_h = \frac{\mathcal{B}(\psi(2S) \rightarrow h)}{\mathcal{B}(J/\psi \rightarrow h)}$ are also given.

| Channel ($\psi(2S) \rightarrow$) | $n^{sig.}$ | ϵ (%) | $\mathcal{B}_{\psi(2S) \rightarrow} (\times 10^{-4})$ | $\mathcal{B}_{J/\psi \rightarrow} (\times 10^{-4})$ | $\frac{\mathcal{B}(\psi(2S))}{\mathcal{B}(J/\psi)} (%)$ |
|---|--------------|----------------|---|---|---|
| $\gamma\eta\pi^+\pi^-^a$ | 418 \pm 60 | 8.69 | 8.71 \pm 1.25 \pm 1.64 | - | - |
| $\gamma\eta\pi^+\pi^-^b$ | - | - | 3.60 \pm 1.42 \pm 1.83 | 39 \pm 7.3 [14] | 9.2 \pm 6.2 |
| $\gamma\eta'(958)$ | 23 \pm 5 | 7.58 | 1.24 \pm 0.27 \pm 0.15 | 43.1 \pm 3 | 2.9 \pm 0.7 |
| $\gamma\eta(1405) \rightarrow \gamma\eta\pi^+\pi^-$ | 10 \pm 7 | 5.06 | 0.36 \pm 0.25 \pm 0.05 | 3.0 \pm 0.5 | 12 \pm 10 |
| | < 24 | 5.06 | < 1.0 | 3.0 \pm 0.5 | < 33 |
| $\gamma\eta(1475) \rightarrow \gamma\eta\pi^+\pi^-$ | < 20 | 4.80 | < 0.83 | 3.0 \pm 0.5 | < 28 |
| $\gamma\eta(1405) \rightarrow \gamma K \bar{K} \pi^c$ | < 11 | 4.54 | < 0.8 | 28 \pm 6 | < 2.9 |
| $\gamma\eta(1475) \rightarrow \gamma K \bar{K} \pi^c$ | < 16 | 4.58 | < 1.5 | 28 \pm 6 | < 5.4 |
| $\gamma\eta(1405) \rightarrow \gamma K \bar{K} \pi^d$ | < 9 | 3.63 | < 1.3 | 28 \pm 6 | < 4.6 |
| $\gamma\eta(1475) \rightarrow \gamma K \bar{K} \pi^d$ | < 9 | 3.54 | < 1.4 | 28 \pm 6 | < 5.0 |

^a all processes in the $\psi(2S) \rightarrow \gamma\eta\pi^+\pi^-$;

^b all processes excluding $\psi(2S) \rightarrow \gamma\chi_{c1} \rightarrow \gamma\eta\pi^+\pi^-$;

^c the decay mode is $\gamma K_S^0 K^+ \pi^- + c.c.$;

^d the decay mode is $\gamma K^+ K^- \pi^0$.

corresponding J/ψ branching fractions [2], as well as the ratio Q_h of $\psi(2S)$ to J/ψ branching fractions for each channel. Decay of $\psi(2S)$ to $\gamma\eta\pi^+\pi^-$ is consistent with the 12% rule expectation within errors; decays of $\psi(2S)$ to $\gamma\eta(1405) \rightarrow \eta\pi^+\pi^-$ and $\gamma\eta(1475) \rightarrow \eta\pi^+\pi^-$ cannot be tested because of low statistics; while the other modes are suppressed by a factor of 2 \sim 4. The $\psi(2S) \rightarrow \gamma\eta'(958)$ branching fraction with $\eta'(958) \rightarrow \eta\pi^+\pi^-$ is more precise than $(2.00 \pm 0.59 \pm 0.29) \times 10^{-4}$ measured by BES I [15].

No signal for $\eta(1405)/\eta(1475)$ is observed in either

$\gamma K_S^0 K^+ \pi^- + c.c.$ or $\gamma K^+ K^- \pi^0$ final states. There is a small peak at 1430 MeV/ c^2 in the $\gamma\eta\pi^+\pi^-$ final state, and we have treated it as $\eta(1405)$ signal. Because of its low statistics, we also set the upper limit at the 90% C.L. for $\psi(2S) \rightarrow \gamma\eta(1405)/\eta(1475) \rightarrow \gamma\eta\pi^+\pi^-$. As shown in Table II, the upper limits at the 90% C.L. on $\psi(2S) \rightarrow \gamma\eta(1405)/\eta(1475) \rightarrow \gamma K \bar{K} \pi$ and $\gamma\eta\pi^+\pi^-$ are at the same level $0.8 \sim 2.0 \times 10^{-4}$.

In the above study in the high $\eta\pi^+\pi^-$ mass region, only χ_{c1} is considered. If we fit $m_{\eta\pi^+\pi^-}$ with $\chi_{c0,1,2}$ together, the fit yields -32 ± 28 , 250 ± 32 , and

TABLE III: Branching fractions for $\chi_{cJ} \rightarrow K_S^0 K^+ \pi^- + c.c.$ and $\chi_{cJ} \rightarrow \eta \pi^+ \pi^-$. Here $\mathcal{B}(\psi(2S) \rightarrow \gamma \chi_{c0}) = (8.6 \pm 0.7)\%$, $\mathcal{B}(\psi(2S) \rightarrow \gamma \chi_{c1}) = (8.4 \pm 0.8)\%$ and $\mathcal{B}(\psi(2S) \rightarrow \gamma \chi_{c2}) = (6.4 \pm 0.6)\%$ are used in the calculation.

| Channel | χ_{cJ} | $n^{sig.}$ | ε (%) | $\mathcal{B}(\times 10^{-3})$ | BESI ($\times 10^{-3}$) |
|--------------------------|-------------|----------------|-------------------|-------------------------------|---------------------------|
| $K_S^0 K^+ \pi^- + c.c.$ | χ_{c0} | < 10 | 6.24 | < 0.3 | < 0.71 |
| | χ_{c1} | 220 ± 16 | 6.80 | $4.1 \pm 0.3 \pm 0.7$ | $2.46 \pm 0.44 \pm 0.65$ |
| | χ_{c2} | 28.4 ± 7.6 | 5.82 | $0.8 \pm 0.3 \pm 0.2$ | < 1.06 |
| $\eta \pi^+ \pi^-$ | χ_{c0} | < 32 | 6.64 | < 1.2 | - |
| | χ_{c1} | 222 ± 28 | 7.90 | $6.1 \pm 0.8 \pm 1.0$ | - |
| | χ_{c2} | < 48 | 7.17 | < 2.2 | - |

TABLE IV: Branching fractions of $\chi_{c1} \rightarrow K^* \bar{K}$, $a_0(980)\pi$ and $f_2(1270)\eta$. Here $\mathcal{B}(\psi(2S) \rightarrow \gamma \chi_{c1}) = (8.4 \pm 0.8)\%$ is used in the calculation.

| Channel | $n^{sig.}$ | ε (%) | $\mathcal{B}(\times 10^{-3})$ |
|---|-----------------|-------------------|-------------------------------|
| $K^*(892)^0 \bar{K}^0 + c.c.$ | 22.5 ± 7.3 | 7.67 | $1.1 \pm 0.4 \pm 0.2$ |
| $K^*(892)^+ K^- + c.c.$ | 26.7 ± 11.0 | 6.20 | $1.6 \pm 0.7 \pm 0.3$ |
| $K_J^*(1430)^0 \bar{K}^0 + c.c. \rightarrow K_S^0 K^+ \pi^- + c.c.$ | < 41 | 6.28 | < 1.0 |
| $K_J^*(1430)^+ K^- + c.c. \rightarrow K_S^0 K^+ \pi^- + c.c.$ | < 79 | 5.00 | < 2.5 |
| $a_0(980)^+ \pi^- + c.c. \rightarrow \eta \pi^+ \pi^-$ | 58 ± 14 | 6.10 | $2.0 \pm 0.5 \pm 0.5$ |
| $f_2(1270)\eta$ | 53 ± 13 | 6.55 | $2.1 \pm 0.5 \pm 0.4$ |

17 ± 26 for χ_{c0} , χ_{c1} , and χ_{c2} , respectively. The difference in the number of χ_{c1} events is 2.3%, which has been taken into account as a systematic error. The 90% C.L. upper limits on the number of χ_{c0} and χ_{c2} events are calculated to be 32 and 48, and the relative systematic errors are 12.4% and 13.3%, respectively. The corresponding upper limits at the 90% C.L. on the branching fractions are listed in Table III.

For the $\chi_{cJ} \rightarrow K_S^0 K^+ \pi^- + c.c.$ decays (listed in Table III), we get higher precision results compared to the BES I experiment [8]. The branching fraction of $\chi_{c1} \rightarrow K_S^0 K^+ \pi^- + c.c.$ is consistent with the BES I result within 1σ , while the results for $\chi_{cJ} \rightarrow \eta \pi^+ \pi^-$ decays are all first measurements. The branching fractions of χ_{c1} decays into intermediate processes listed in Table IV are all also first observations.

χ_{c0} is forbidden to decay into $K \bar{K} \pi$ or $\eta \pi^+ \pi^-$ by spin-parity conservation, and only upper limits at the 90% C.L. are determined for these branching fractions. For χ_{cJ} decay into hadrons in lowest-order,

χ_{c1} decay is suppressed by a factor α_s compared with χ_{c2} decay. However, the branching fractions of χ_{c1} decays into $K \bar{K} \pi$ and $\eta \pi^+ \pi^-$ are both much larger than those of χ_{c2} decays. This result needs explanation.

Acknowledgments

The BES collaboration thanks the staff of BEPC for their hard efforts. This work is supported in part by the National Natural Science Foundation of China under contracts Nos. 19991480, 10225524, 10225525, the Chinese Academy of Sciences under contract No. KJ 95T-03, the 100 Talents Program of CAS under Contract Nos. U-11, U-24, U-25, and the Knowledge Innovation Project of CAS under Contract Nos. U-602, U-34 (IHEP); by the National Natural Science Foundation of China under Contract No. 10175060 (USTC); and by the Department of Energy under Contract No. DE-FG03-94ER40833 (U Hawaii).

[1] BES Collab., M. Ablikim *et al.*, Phys. Rev. D **73**, 052004 (2006); BES Collab., M. Ablikim *et al.*, Phys. Rev. D **72**, 012002 (2005); BES Collab., M. Ablikim *et al.*, Phys. Rev. D **71**, 072006 (2005); BES Collab., M. Ablikim *et al.*, Phys. Lett. B **619**, 247 (2005); BES Collab., M. Ablikim *et al.*, Phys. Lett. B **614**, 37 (2005); BES Collab., J. Z. Bai *et al.*, Phys. Rev.

Lett. **92**, 052001 (2004); BES Collab., M. Ablikim *et al.*, Phys. Rev. D **70**, 112007 (2004); BES Collab., M. Ablikim *et al.*, Phys. Rev. D **70**, 112003 (2004); BES Collab., J. Z. Bai *et al.*, Phys. Rev. D **69**, 072001 (2004); CLEO Collab., N. E. Adam *et al.*, Phys. Rev. Lett. **94**, 012005 (2005); CLEO Collab., T. K. Pedlar *et al.*, Phys. Rev. D **72**, 051108 (2005); CLEO Col-

- lab., R. A. Briere *et al.*, Phys. Rev. Lett. **95**, 062001 (2005).
- [2] Particle Data Group, S. Eidelman *et al.*, Phys. Lett. B **592**, 1 (2004).
- [3] T. Appelquist and H. D. Politzer, Phys. Rev. Lett. **34**, 43 (1975); A. De Rujula and S. L. Glashow, *ibid*, page 46.
- [4] L. Köpke and N. Wermes, Phys. Rep. **174**, 67 (1989).
- [5] L3 Collab., M. Acciarri *et al.*, Phys. Lett. B **501**, 4111 (2001).
- [6] CLEO Collab., R. Ahohe *et al.*, Phys. Rev. D **71**, 072001 (2005).
- [7] D.L. Scharre *et al.*, Phys. Lett. **97B**, 329 (1980).
- [8] BES Collab., J. Z. Bai. *et al.*, Phys. Rev. D **60**, 072001 (1999).
- [9] BES Collab., J. Z. Bai *et al.*, Nucl. Instr. Meth. A **458**, 627 (2001).
- [10] The significance S is estimated with the formula $S = \sqrt{-2 \times (\ln L_2 - \ln L_1)}$, where L_1 and L_2 is the likelihood value in the fit with and without signal, respectively.
- [11] As an example, for $K_2^*(1430)^0$, the fits under different hypotheses yield: 15.9 ± 7.1 , 21.8 ± 14.7 and 18.6 ± 11.5 for $K_2^*(1430)$, $K_0^*(1430)$ and $K^*(1410)$, respectively. So the biggest number is $21.8 + 14.7 = 36.5$, the smallest number is $18.6 - 11.5 = 7.1$, then the mean is $(36.5 + 7.1)/2 = 21.8$, the error is $36.5 - 21.8 = 14.7$, and the average number of events is 22 ± 15 .
- [12] BES Collab., M. Ablikim *et al.*, Nucl. Instrum. Meth. A **552**, 344 (2005).
- [13] Mark-I Collab., W. Tanebaum *et al.*, Phys. Rev. D **17** 1731 (1978); G. Karl, S. Meshkov, and J. L. Rosner, Phys. Rev. D **13**, 1203 (1976); Crystal Ball Collab., M. Oreglia *et al.*, *ibid*, **25**, 2259 (1982).
- [14] C. Edwards, *et al.*, Phys. Rev. Lett. **51**, 859 (1983).
- [15] BES Collab., J. Z. Bai *et al.*, Phys. Rev. D **58**, 097101 (1998).